Dielectric, infrared, and Raman response of undoped $SrTiO_3$ ceramics: Evidence of polar grain boundaries

J. Petzelt,[1] T. Ostapchuk,[1] I. Gregora,[1] I. Rychetský,[1] S. Hoffmann-Eifert,[2] A. V. Pronin,[5] Y. Yuzyuk,[4,*] B. P. Gorshunov,[3,5] S. Kamba,[1] V. Bovtun,[1] J. Pokorný,[1] M. Savinov,[1] V. Porokhonskyy,[1] D. Rafaja,[6] P. Vaněk,[1] A. Almeida,[4] M. R. Chaves,[4] A. A. Volkov,[5] M. Dressel,[3] and R. Waser[2]

[1]*Institute of Physics, Academy of Sciences of the Czech Republic, Na Slovance 2, 18221 Prague 8, Czech Republic*

[2]*Institut f. Festkörperforschung Jülich, D-52425 Jülich, Germany*

[3]*Physikalisches Institut, Universität Stuttgart, D-70550 Stuttgart, Germany*

[4]*Departamento de Fisica, IFIMUP, Faculdade de Ciencias da Universidade do Porto, Rua do Campo Alegre 687, 4169-007, Portugal*

[5]*Institute of General Physics, RAS, 119991 Moscow, Russian Federation*

[6]*Faculty of Mathematics and Physics, Charles University, Ke Karlovu 3, 121 16 Praha 2, Czech Republic*

(Received 5 June 2001; published 22 October 2001)

Thorough Raman and infrared (IR) reflectivity investigations of nominally pure $SrTiO_3$ ceramics in the 10–300 K range have revealed a clear presence of the polar phase whose manifestation steeply increases on cooling. The Raman strengths of the Raman-forbidden IR modes are proportional to $\omega_{TO1}^{-\alpha}(\alpha \approx 1.6)$ where ω_{TO1} is the polar soft mode frequency. No pronounced permittivity dispersion is observed below the soft mode frequency so that, as in single crystals, the static permittivity is essentially determined by the soft mode contribution. A theory is suggested which assumes a frozen dipole moment connected with the grain boundaries which induces the polar phase in the grain bulk in correlation with the bulk soft-mode frequency. This stiffens slightly the effective soft mode response and reduces the low-temperature permittivity compared to that of single crystals. Moreover, the polar soft mode strongly couples to the E_g component of the structural soft doublet showing that the polar axis is perpendicular to the tetragonal axis below the structural transition which is shifted to 132 K in our ceramics. Whereas the TiO_6 octahedra tilt (primary order parameter) below the structural transition corresponds to that in single crystals, much smaller A_{1g}-E_g splitting of the structural soft doublet shows that the tetragonal deformation (secondary order parameter) is nearly 10 times smaller, apparently due to the grain volume clamping in ceramics.

DOI: 10.1103/PhysRevB.64.184111 PACS number(s): 63.20.−e, 68.35.Rh, 78.30.−j, 77.22.−d

I. INTRODUCTION

Strontium titanate $SrTiO_3$ (STO) has been one of the most popular materials since the discovery of its incipient ferroelectricity and first polar soft mode behavior.[1] Owing to its high dielectric permittivity, that increases on cooling, and to its low microwave (MW) losses it is the most attractive material for many high-frequency and MW applications, particularly at low temperatures.[2–4] For this reason, great attention has been paid recently to dielectric properties of STO thin films which, however, show dramatic differences compared to bulk samples. The permittivity is much smaller and thickness dependent, its increase on cooling saturates at higher temperatures[5–7] and, correspondingly, the polar mode softening levels off at much higher frequencies.[8–11] Several reasons affecting this behavior were discussed: influence of a low-permittivity (dead) layer at the electrode-film interface,[5,6,12–14] stress caused by the mismatch with the substrate,[14,15] nonstoichiometry, porosity, and granularity.[12,14,16] However, so far it has not been clear which of these effects (if any) predominates. To simplify the situation and eliminate all the effects but grain boundaries (and possible point defects), we decided to study a nominally pure bulk STO ceramics.

Unlike single crystals, surprisingly little attention has been so far paid to pure STO ceramics. Earlier literature reports on dielectric data including the MW range,[2,3] and show that, as in single crystals, there is no appreciable dielectric dispersion present down to low temperatures (about 50 K) up to the 10^{10} Hz range. However, the permittivity values at liquid He temperatures are several times smaller in ceramics (a few thousands) than in good single crystals, where they reach about 25 000,[17,18] and the MW losses in ceramics are also appreciably higher and grain size dependent.[2,3] No soft mode studies on STO ceramics are known to the authors, even if it is clear (via Lyddane-Sachs-Teller relations) that the lower permittivity values should imply a smaller softening (higher frequency) of the soft mode. This paper reports on our Raman, IR and submillimeter (SMM) reflectivity, and SMM transmission measurements (complemented by MW and rf dielectric measurements), which confirmed this effect, and also brought clear evidence for the existence of polar regions in STO ceramics. A theory is suggested to explain the appearance of polar regions and the soft mode stiffening through the dipoles (polarization) frozen at the grain boundaries. Some of our data have been briefly published recently.[10,19,20]

II. EXPERIMENTAL

The STO ceramics samples were prepared by a conventional mixed-oxide route[21] starting from high-purity $SrCO_3$ (Selectipur, Merck, Darmstadt, FRG) and fine grained TiO_2 powder (TM-1, Fuji, Koygo, Japan). The stoichiometry of the samples was adjusted to $Sr_{1.000}Ti_{1.001}O_3$ by mixing of the

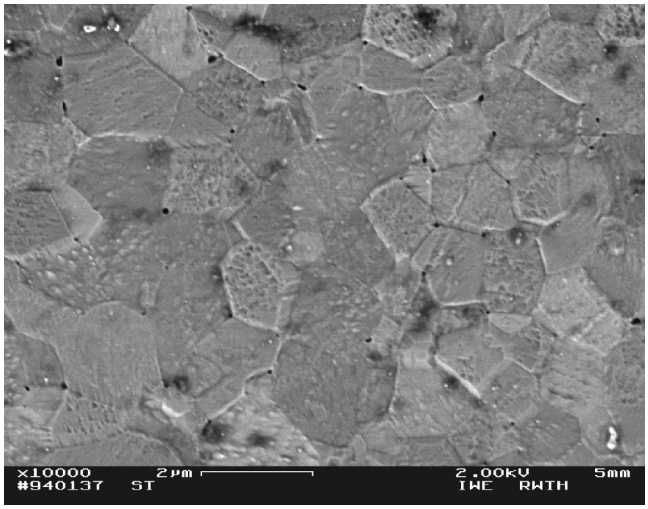

FIG. 1. SEM micrograph of the polished STO ceramics surface.

right amounts of the precursor powders. The powders were mixed in a cyclohexanolic suspension for 1 h, ball milled for 3 h and subsequently calcined at 1050 °C for 18 h. The formation of perovskite phase was checked by XRD. Cold-pressed cylinders of STO were sintered at 1380 °C for 7 h. The single-phase samples exhibit a density of about 5.05 g/cm^3, i.e., 98.8% of the theoretical density. The mean grain size of the ceramics, of around 1–2 μm, was determined from SEM analysis of polished samples (see Fig. 1).

The impurity content was determined by means of inductive coupled plasma induced atomic emission spectroscopy (ICP-AES). The concentration of heterovalent impurities (e.g., Al, Fe, K, Na, Nb) was below 150 mol ppm, homovalent impurities of Ba (427 mol ppm) and Ca (2500 mol ppm) originate from the precursor powder, contamination with Si (150 mol ppm), Y (110 mol ppm) and Zr (2100 mol ppm) is caused by the milling process. Such an impurity level (particularly Ca) may lead to an increase of the low-temperature permittivity in single crystals,[22,23] but does not change the phase diagram appreciably (particularly it does not induce the ferroelectric transition). The samples were mechanically polished with alumina slurry and chemically polished with Synthon (fluoride based SiO_2 slurry). Since in the case of STO single crystals it is now well established that the surface treatment plays an important role in the dielectric[5] as well as x-ray and neutron scattering experiments,[24,25] we decided to also pay attention to this problem in the case of ceramics. Some of the samples were etched for about 1 h in boiling (130 °C) concentrated orthophosphoric acid to remove a layer of a few μm in thickness from the surface.[5,18]

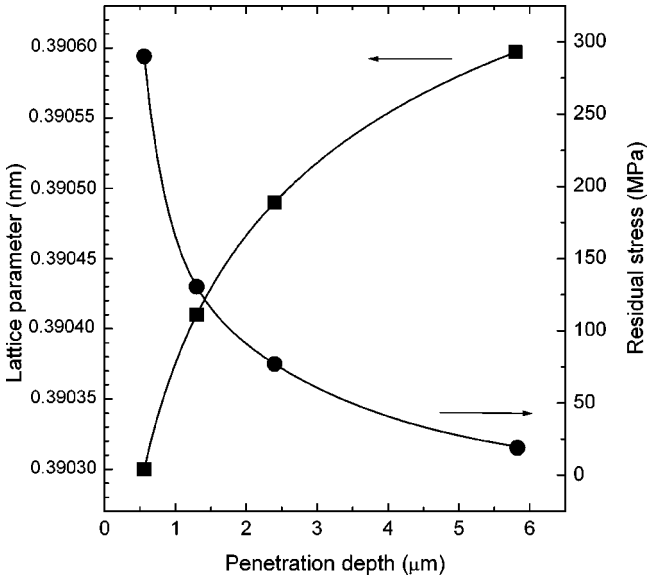

FIG. 2. Stress-free lattice parameter and residual stress of the STO ceramics as a function of the mean penetration depth of x rays.

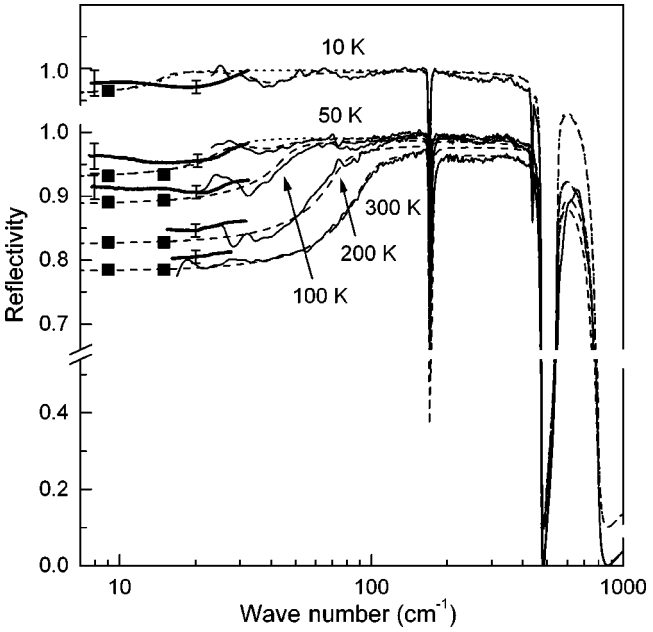

FIG. 3. IR reflectivity of the STO ceramics together with measured BWO reflectivity (thick full lines), calculated reflectivity from BWO transmission (full squares) and multioscillator fits (dotted lines—without the *X* mode, dashed lines—including the *X* mode) at selected temperatures.

Real structure of our samples was investigated at room temperature both in symmetrical and in asymmetrical diffraction geometry. The symmetrical scans were performed with a Bragg-Brentano diffractometer; the asymmetrical scans have been done at glancing angles of incidence using the parallel beam optics. The asymmetrical diffraction geometry enabled the structure to be investigated at different depths below the sample surface and to determine the residual stresses (macroscopic deformation of the crystal lattice). The presence of the structural phase transition was investigated by differential thermal analysis (DTA) using Perkin-Elmer DSC-7 calorimeter. However, unlike in a single crystal, no transition could be detected.

Standard dielectric measurements in the 10^2–10^6 Hz range (impedance analyzer Hewlett-Packard 4192A) revealed the usual dispersionless permittivity values with a monotonic increase on cooling and a saturated value of almost 10 000 at 10 K. MW measurements at 36.2 GHz were performed from 300 to 90 K using the impedance measure-

TABLE I. Fitted IR (TO and LO) and first-order Raman frequencies at selected temperatures. The numbers in parentheses indicate the corresponding damping. All numbers are in cm^{-1}.

	15 K		50 K		100 K		300 K	
	IR	Raman	IR	Raman	IR	Raman	IR	Raman
TO_1	15 (2)	15	26 (6)	29 (20)	46 (9)	45 (17)	93 (20)	~88 (20)
LO_x TO_x	38 (17) 42 (18)	40 (18)	37 (18) 41 (18)	~38 (19)				
A_{1g}(soft)		52 (13)		50 (14)		36 (15)		
E_g+B_{1g} (R'_{25})		144 (4)		145 (4)		144 (5)		
LO_1 TO_2	169 (0.3) 172 (0.5)	171 (4)	169 (0.3) 172 (0.5)	172 (4)	169 (0.3) 173 (0.6)	172 (5)	171 (1.1) 176 (3)	175 (6)
B_{2g} (R_{12})		229 (7)		~230 (8)				
TO_3, LO_3 (F_{2u} silent)		~263 (5)						
LO_R E_u, (R_{15})	435 (6)		435 (8)					
TO_R E_u, (R_{15})	436 (6)		436 (9)					
E_g+B_{1g} (R'_{25})		447 (4)		447 (4)		446 (5)		
LO_2	473 (2)	478 (8)	474 (2)	478 (9)	473 (2)		472 (2)	
TO_4	548 (7)	546 (7)	548 (7)	545 (8)	548 (7)	545 (9)	548 (11)	~546 (15)
LO_4 A_{2g} (R_1)	795 (26)	795 (25)	795 (26)	796 (26)	795 (26)	796 (28)	795 (35)	~797 (40)

ments of a section of shorted rectangular waveguide with the sample mounted at one end.[19] The IR reflectivity measurements (20–650 cm^{-1}, 10–300 K) were carried out using Bruker IFS 113v Fourier transform spectrometer equipped with pyroelectric DTGS room-temperature detector as well as cooled (1.5 K) Si bolometer. In addition, SMM reflectivity (15–25 cm^{-1}, 300–5 K) was measured on the same etched sample using a coherent-source [based on backward wave oscillators (BWO's)] millimeter-submillimeter spectrometer[26] in a special reflectance mode. Using a similar technique, we also succeeded to measure the SMM complex transmission spectra (8–15 cm^{-1}, 300–5 K) on a very thin (24 μm thick) polished and etched plane-parallel platelet.

The unpolarized Raman spectra were taken using the 514.5 nm line of an Ar^+ Coherent Innova 90 laser and a Jobin Yvon T64000 spectrometer with CCD and photon counting detector in a pseudo back-scattering geometry in the 15–300 K temperature and 20–1000 cm^{-1} frequency range. Subtractive mounting with multichannel CCD detection as well as additive mounting (better resolution and extended low-frequency range) with single-channel photon counting was used. The spectral resolution was about 3 and 2 cm^{-1}, respectively. Basically the same features as will be reported here (particularly the appearance of the forbidden IR modes) were confirmed also with several other STO ceramic samples of various origins and surface treatment (polishing, etching) using a micro-Raman spectrometer (Renishaw Ramascope) at 300–80 K.

III. RESULTS

The Rietveld analysis of the x-ray diffraction pattern measured in the symmetrical mode confirmed the phase purity with no detectable preferred orientation of crystallites and yielded the cubic lattice parameter $a=0.390597 \pm 0.000003$) nm in the direction normal to the sample surface. This value is close to that of ideal STO structure (0.39050 nm) and the small difference may be influenced by residual stresses or slight nonstoichiometry. Detailed analysis of diffraction profiles has shown that the crystallite size is comparable with the grain size as obtained from SEM. From this comparison, we can draw a particular conclusion that the individual grains are single crystalline. The asymmetric diffraction enabled us to determine[27] the residual stress and the stress-free lattice parameters as a function of the mean penetration depth (Fig. 2). For the angles of incidence 2°, 5°, and 10°, the penetration depths in STO are 0.56, 1.3, and 2.4 μm, respectively. They are nearly independent of the diffraction angle. The same results (concerning the depth gradient of the stress-free lattice parameter and that of the residual stress) were obtained on the polished and on etched surface. The small surface gradient of the stress-free lattice parameter may be caused by some surface nonstoichiometry (e.g. oxygen vacancies) which may be limited to much thinner layer (few atomic layers) than indicated in Fig. 2, due to the finite penetration depth over which the values in Fig. 2 are averaged.

In Fig. 3 we show our IR reflectivity including the SMM data. Our previously published IR spectra of STO ceramics[10,19] indicated features not typical for the crystalline STO.[1,8] In order to obtain true results in the present experiment we took into account the possible distortion of the spectra caused by polishing of its surface. We have established that FIR spectra of the etched ceramics give more

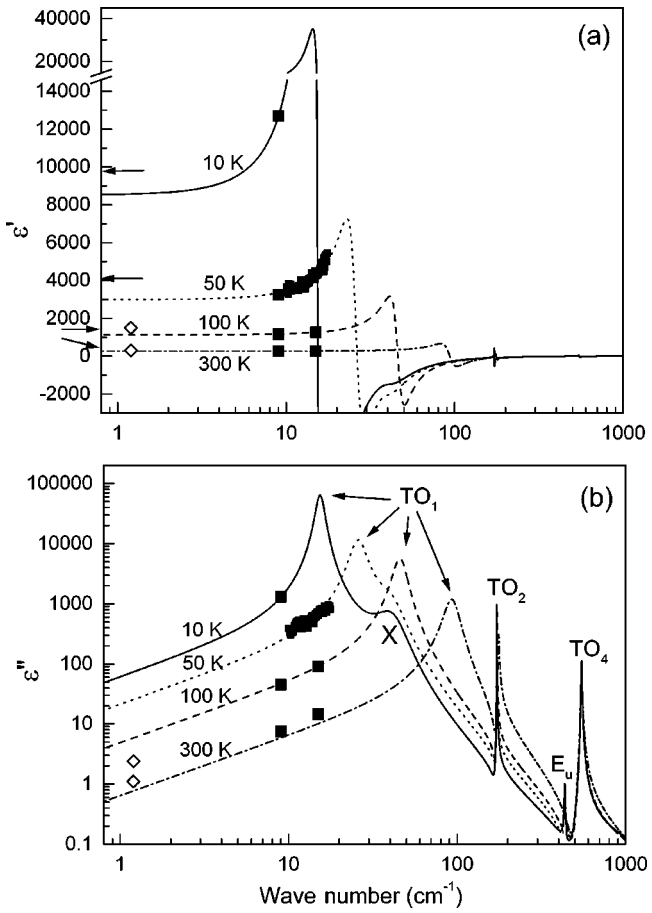

FIG. 4. Dielectric permittivity (a) and loss (b) spectra calculated from the reflectivity fits (lines) together with measured BWO transmission and MW data (full squares and open diamonds, respectively). Arrows indicate the measured low-frequency permittivity.

reasonable results in the 25–300 cm^{-1} range than those of the polished one. At higher frequencies the roughness of the etched surface leads, however, to a decrease of the reflectance. In this respect the spectra presented in Fig. 3 were combined from the spectra of the etched sample in the 25–300 cm^{-1} range and polished sample in the 300–650 cm^{-1} range. In order to avoid the problem of geometrical and optical changes of the cryostat on cooling, we performed the reference measurements of the mirror at all the temperatures. The regime was kept the same for both sample and mirror: relatively fast cooling down to 10 K and then measurements on heating.

The IR reflectivity spectra (full line in Fig. 3) were fitted in a standard way with a factorized form of the dielectric function[28] to obtain the polar phonon mode parameters (see Table I). During the fitting procedure we also took into account the reflectivity directly measured by the coherent source technique in the 9–30 cm^{-1} range and the reflectivity calculated from the transmission data obtained by this technique between 9 and 15 cm^{-1}. From the fit parameters the complex dielectric function was calculated and compared with that directly obtained from the SMM transmittance data. Trial and error fitting was used to optimize the agreement between all the data and fit parameters. The imperfect reflectivity fit around 20 cm^{-1} at 10 K is enforced by good fits of the BWO complex permittivity data, which are preferred because of the general higher accuracy of the transmission measurements. In Fig. 4 we show the resulting calculated real ε' and imaginary part ε'' of the dielectric function for selected temperatures. Also the SMM and MW data are shown. In addition to 3 IR-active transverse optic modes TO_1 (soft mode), TO_2, and TO_4 clearly seen at room temperature and the E_u mode activated from the R point of the Brillouin zone below the antiferrodistortive transition temperature T_a due to the Brillouin zone folding, an additional mode (denoted by X) not appearing in single crystals arises near 40 cm^{-1} at low temperatures. In Fig. 3, together with the fit described above (dashed line), we plotted the fitting curve which does not include the X mode at 15–50 K (dotted line). In spite of the experimental inaccuracy, including this mode into the fit model seems to improve the fit and is reasonable from the viewpoint of the Raman data and their

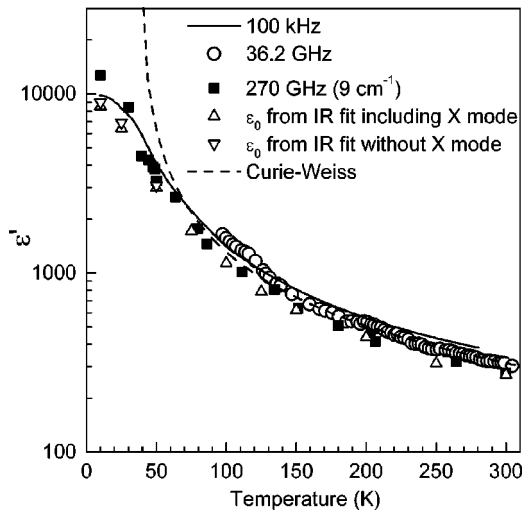

FIG. 5. Temperature dependence of the permittivity at different frequencies compared with the static permittivity data from IR reflectivity fits. The dashed line is the Curie–Weiss fit from Ref. 2.

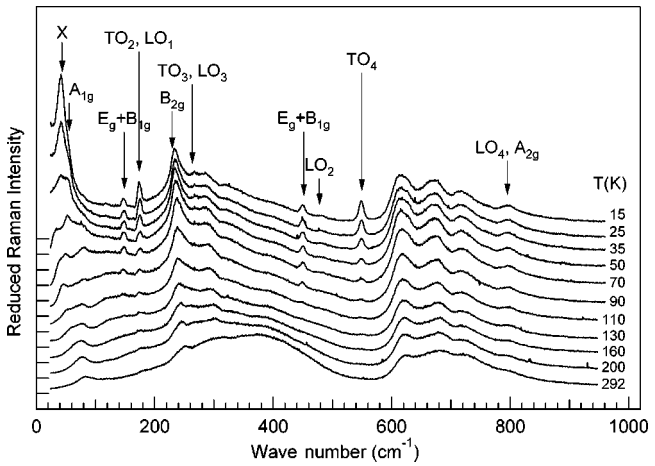

FIG. 6. Overall view of unpolarized Raman spectra of STO ceramics at selected temperatures (reduced multichannel data at lower resolution).

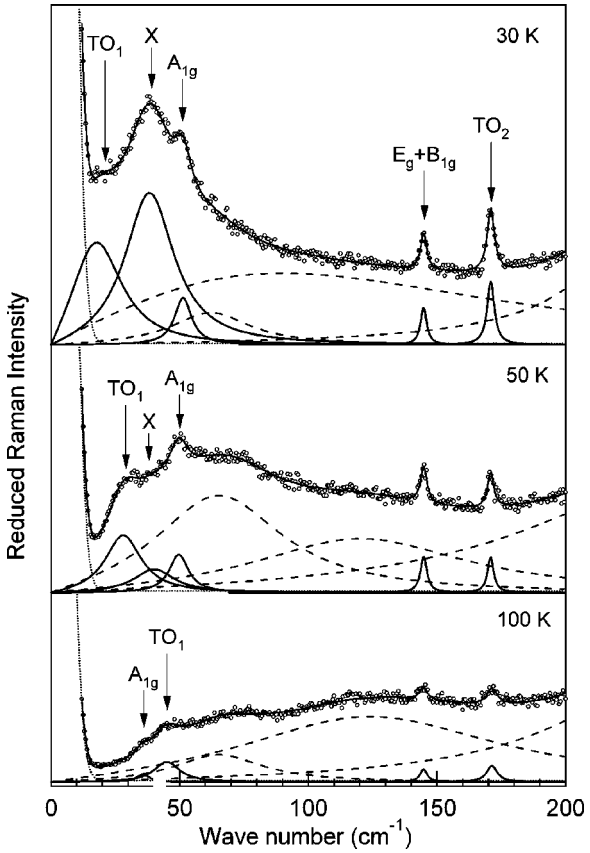

FIG. 7. Low-frequency part of the fit to the Raman data at three selected temperatures (reduced single channel data at higher resolution), showing the resolved single-phonon features (full lines). Dashed peaks simulate the second-order background.

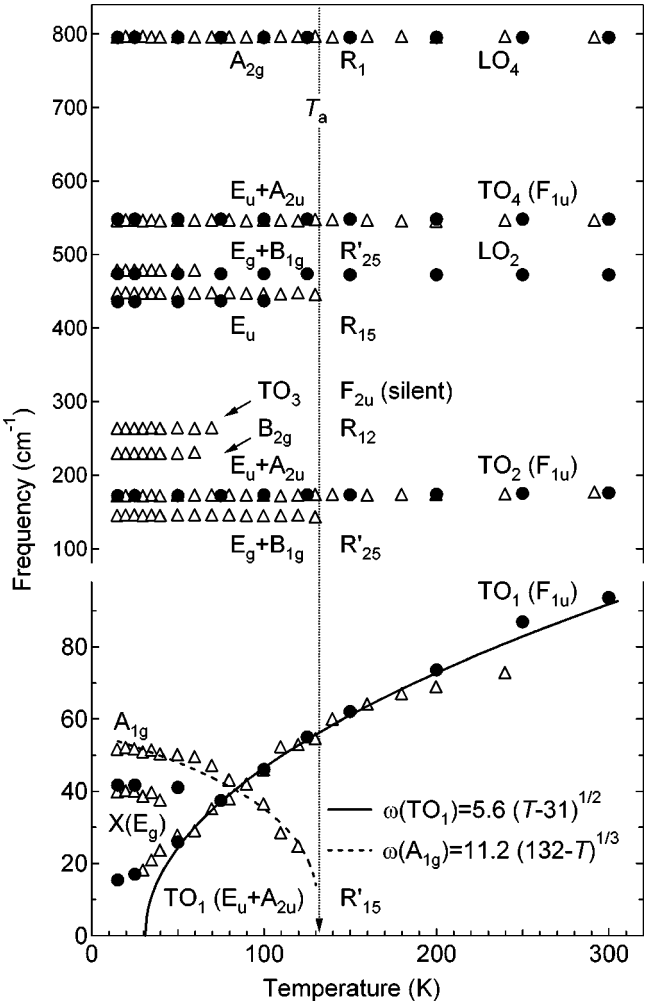

FIG. 8. Temperature dependences of the main observed mode frequencies together with their assignment—comparison of FIR and Raman data.

assignment. The temperature dependence of the experimental permittivity values obtained in various frequency ranges, as well as the static permittivity values from our fit and earlier Curie-Weiss fit to MW data of ceramics[2] are plotted in Fig. 5. The presence of the *X* mode in the fits does appreciably influence the soft-mode dielectric strength, but the total IR contribution to static permittivity is practically the same for both fits.

Selected Raman spectra reduced by the Stokes temperature factor are shown in Fig. 6. As in single crystals,[23,29,30] second-order features dominate the spectra at higher temperatures. On lowering the temperature, however, IR-active modes start to emerge in addition to the folded *R*-point modes. The reduced spectra were carefully fitted with classical damped multioscillator model (including a Gaussian divided by the temperature factor to represent the Rayleigh wing). An example of a fit to the single-channel data in the low-frequency region is illustrated in Fig. 7. We note that several broad peaks were used in the fit only to simulate the structure of strong background due to second-order scattering and are not taken into consideration as one-phonon features.

The behavior of the low-frequency part of the spectra (below $\sim 100\ \mathrm{cm}^{-1}$) on cooling deserves a special comment: First, a weak TO_1 peak splits from a broad second-order feature at $\sim 90\ \mathrm{cm}^{-1}$ and softens. At about 90 K, it crosses the A_{1g} soft mode, which emerges below ~ 130 K from the Rayleigh wing and hardens on cooling. The TO_1 mode continues to soften and can be reliably traced to about 30 K (Fig. 7). Below this temperature, it is no more observable, becoming heavily damped and merging eventually with the Rayleigh wing, whose intensity has markedly increased. Its estimated frequency at lowest temperatures is compatible with the IR data, but the fit requires higher damping. In addition, a mode referred to as *X* starts to appear below some 50 K at $\sim 40\ \mathrm{cm}^{-1}$, gains intensity on cooling and becomes eventually the dominant feature of the low-frequency spectra. The second-order feature at $\sim 80\ \mathrm{cm}^{-1}$ virtually disappears at lowest temperatures.

The temperature dependences of relevant mode frequencies obtained from the IR and Raman data are plotted in Fig. 8 together with their suggested assignment. In Table I we listed the fitted parameters from the IR and Raman data at several temperatures. The temperature dependence of some of the activated *R* point and IR mode Raman strengths (integrated intensities) is shown in Fig. 9. The corresponding fits will be discussed below.

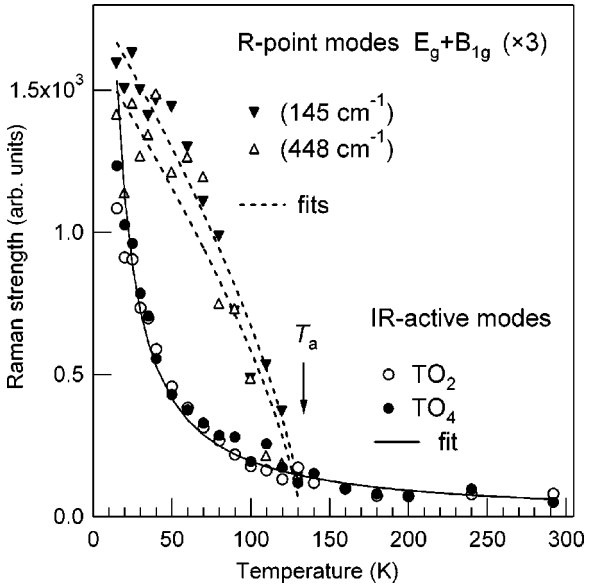

FIG. 9. Temperature dependences of the Raman strengths of the selected *R*-point and IR modes. The dotted lines correspond to $I \propto (T_a - T)^{0.72}$, the full line to $I \propto e^{-aT}$.

IV. DISCUSSION AND THE THEORETICAL MODEL

The results of the group-theoretical analysis of lattice vibrations in both STO phases using published data[30–33] are summarized in Table II. For the analysis in the tetragonal phase we used the system of cubic axes,[31] which results in exchange of B_{1g} and B_{1u} for B_{2g} and B_{2u} representations, respectively, compared to the more commonly used system of tetragonal axes where the *a* and *b* axes are rotated by 45° in the plane normal to the tetragonal *c* axis. In addition the correlation is shown with the two most probable polar phases suggested below and the observed TO mode frequencies at 300 and 15 K together with their symmetry assignment. In general a good agreement between IR and Raman data is seen.

As in single crystals, the ω_{TO1} frequency, from Fig. 8, obeys the classical Cochran softening law $\omega^2_{\mathrm{TO1}} \propto (T - T_0)$ above ~60 K with the extrapolated zero frequency $T_0 \approx 31$ K. Below T_a, the single crystal Raman data display the well-known soft $A_{1g}+E_g$ doublet[30] which saturates at low temperatures near 49 and 15 cm^{-1}, respectively. In our ceramics we see that the behavior of the weak A_{1g} component is in reasonable agreement with the crystal data. Particularly, its frequency roughly follows the power law $\omega(\mathrm{A}_{1g}) \propto (T_a - T)^{\beta}$ with critical index of the order parameter $\beta \approx 1/3$ (see Fig. 8). However, the E_g component is apparently absent in the very low-frequency range. We assign the *X* mode near 40 cm^{-1} to the missing E_g component whose pronounced strengthening and partial hardening is caused by a strong coupling with the TO_1 soft mode. Unfortunately, the limited accuracy of our low-frequency data did not allow us to determine the coupling parameters unambiguously. The temperature dependence of the totally symmetric A_{1g} component shows that the primary order parameter, the TiO_6 octahedra tilt, attains the same spontaneous value as in single crystals. However, the $A_{1g}-E_g$ splitting, which in our case at low temperatures amounts to ~9 cm^{-1} only, measures the secondary order parameter, the tetragonal deformation[31,33] (neglecting the small E_g frequency renormalization caused by the coupling previously mentioned). As both these quantities are proportional to the order parameter squared,[31] it appears that the low-temperature spontaneous tetragonal deformation in our ceramics is an order of magnitude smaller than that in single crystals. This can be explained by volume clamping of individual grains by the surrounding grains below T_a, which strongly limits the tetragonal deformation of each grain in the bulk. This could also explain the absence of any measurable specific heat anomaly in our DTA experiment, whereas in a single crystal a weak anomaly of 2 J mol^{-1} K^{-1} was detected.[36]

The temperature dependences of the Raman strengths of the folded *R*-point modes (see Fig. 9) obey the power law $I_R \propto (T_a - T)^{\gamma}$ with $T_a = 132$ K and $\gamma = 0.72 \pm 0.01$ which agrees well with that observed in single crystals [by symmetry $\gamma = 2\beta$ (Ref. 31)]. As seen from Fig. 9, in contrast to single crystals where $T_a \cong 105$–110 K,[37] in our ceramics $T_a = 132$ K. This shift could be caused by internal stress in our ceramics because hydrostatic pressure is known to increase T_a by ~20 K/GPa.[38] Also the unwanted Ca admixture increases T_a.[23]

Unlike the *R*-point modes, the IR modes have nonzero Raman strength even at room temperature and show a much steeper increase on cooling (exponential increase proportional to e^{aT} see fit in Fig. 9). In view of our analysis below, we tried also a power law fit to correlate these strengths with the TO_1 frequency. A good fit can be achieved with $I_R \propto \omega_{\mathrm{TO1}}^{-\alpha}$, $\alpha = 1.6 \pm 0.06$ as shown in Fig. 10. Also the TO_1 mode strength was tentatively estimated by integrating our reduced Raman strength from 12 to 100 cm^{-1}. One can see that except for temperatures below 35 K, where the soft mode response merges with our unresolved central line, this strength obeys the same law as that of TO_2 and TO_4 modes. The appearance of forbidden polar modes in our Raman spectra demonstrates the local loss of the inversion center. Similar symmetry breaking, but only at much lower temperatures, was already observed in Ca doped[23] and O[18] isotope exchanged STO single crystals,[39] in thin films[40] and even in nominally pure STO crystals[41] and was assigned to ferroelectric fluctuations. The bilinear coupling of the TO_1 soft mode to the E_g component only (not to the A_{1g} one in the case of our ceramics) requires by symmetry arguments a polar phase with the polarization perpendicular to tetragonal *c* axis. The two possibilities suggested in Table II with polarization along (110) and (100) directions can be, from the symmetry point of view, realized by the simplest Landau-type equitranslational phase transitions.[42]

Our explanation of polar phase appearance is based on an assumption that at grain boundaries a frozen polarization P_f (dipole moment) exists independent of temperature. This is a plausible assumption since the recent careful studies of a STO bicrystal and ceramics have shown that the structure of the grain boundary is well defined, insulating and sufficiently asymmetric and nonstoichiometric to be connected with a dipole moment.[43–47] Another origin of P_f could be in local-

TABLE II. Symmetry classification of relevant vibrational modes in STO in various phases (including the suggested polar phases), together with our observed IR TO and Raman mode frequencies at 300 and 15 K. The 300 K data for the silent F_{2u} and R'_{15} mode are taken from hyper-Raman (HR) (Ref. 34) and inelastic neutron (N) (Ref. 35) experiments on single crystals, respectively. The frequencies in the last column (observed in Raman) are compatible with the polar symmetry only. All frequencies are in cm^{-1}.

$Pm\bar{3}m$ (O_h^1) Z = 1 ($P_S=0$, T=300 K)			$I4/mcm$ (D_{4h}^{18}) $Z_{prim}=2$ ($P_S=0$, T=15 K)			$F2_{xy}m_{\bar{x}y}m_z$ (C_{2v}^{18}) $Z_{prim}=2$ ($P_x=P_y\neq 0$, T=15 K)		$I2_xm_ym_z$ (C_{2v}^{22}) $Z_{prim}=2$ ($P_x\neq 0$, T=15 K)		
species	activity	observed	species	activity	observed	species	activity	species	activity	observed
$3F_{1u}$	IR	93,176,548	$3A_{2u}$ $3E_u$	IR	15,172,548	$3B_2$ $3A_1+3B_1$	IR + R	$3B_2$ $3A_1+3B_1$	*IR+R*	~15,171,547
$1F_{2u}$	HR	266	$1B_{2u}$ $1E_u$	- IR	- -	$1B_2$ $1A_1+1B_1$	IR + R	$1A_2$ $1A_1+1B_1$	*R* IR + R	~263
$1R'_{15}(F_{1g})$	N	~40 (soft)	$1A_{1g}$ $1E_g$	*R*	52 40	$1A_1$ $1A_2+1B_2$	IR + R	$1A_1$ $1A_2+1B_2$	IR + R	42
$2R'_{25}(F_{2g})$	-	-	$2B_{1g}$ $2E_g$	*R*	144,447	$2A_1$ $2A_2+2B_2$	IR + R	$2B_1$ $2A_2+2B_2$	IR + R	-
$1R_{15}(F_{1u})$	-	-	$1A_{1u}$ $1E_u$	- IR	- 436	$1A_2$ $1A_1+1B_1$	R IR + R	$1A_2$ $1A_1+1B_1$	R IR + R	-
$1R_{12}(E_g)$	-	-	$1A_{2g}$ $1B_{2g}$	- *R*	- 229	$1B_1$ $1B_1$	IR + R	$1B_1$ $1A_1$	IR + R	-
$1R_1(A_{1g})$	-	-	$1A_{2g}$	-	-	$1B_1$	IR + R	$1B_1$	IR + R	795
Total (Γ point)	$3F_{1u}+1F_{2u}$		$1A_{1g}+1A_{1u}+2A_{2g}+3A_{2u}+$ $+2B_{1g}+2B_{2g}+2B_{2u}+3E_g+3E_u$			$8A_1+4A_2+8B_1+7B_2$		$7A_1+5A_2+9B_1+6B_2$		
Mode activity	3 IR		8IR+7*R*			23(IR+*R*)+4*R*		22(IR+*R*)+5*R*		

ized point defects, e.g., O vacancies or Ca impurities whose concentration at grain boundaries could be much higher than the average one. The frozen polarization $P(\mathbf{r})=P_f(\mathbf{r})$, where $\mathbf{r}$ goes through all defects and grain boundaries depends in general on position. The defect-free bulk we describe by the simple Landau-Ginzburg free-energy density functional (valid at least above T_a)

$$f(\mathbf{r})=\frac{a(T-T_0)}{2}P^2+\frac{b}{4}P^4+\kappa(\nabla P)^2, \qquad (1)$$

where T_0 is the extrapolated Curie temperature ($T_0=31$ K in our case).

The inhomogeneous polarization in a small ferroelectric particle[48] (possibly also in the vicinity of point, linear or planar polar defects) can be calculated by minimizing the free energy under the appropriate boundary conditions. The polarization inside a thin slab (approximating roughly a cubic grain with two polar surfaces against each other), for instance, can be expressed as

$$P(x)=P_f\frac{\cosh(x/\xi)}{\cosh(D/2\xi)} \approx P_f\left[\exp\left(-\frac{x+D/2}{\xi}\right)+\exp\left(\frac{x-D/2}{\xi}\right)\right], \qquad (2)$$

where $T>T_0$, P_f is the surface polarization, x is the space coordinate normal to the slab ($x=0$ in the slab center), D its thickness which is much larger than the correlation length $\xi=[a(T-T_0)/\kappa]^{1/2}$ of the polarization fall-off, and ξ is found to be proportional to $\omega_{\mathrm{TO1}}^{-1}$. In our model, the average polarization $P_{\mathrm{av}}\approx 2P_f\xi/D\propto(T-T_0)^{-1/2}$ is proportional to ξ, but in general, assuming the interdefect distances are substantially larger than ξ, one can show that $P_{\mathrm{av}}\propto\xi^d$ where d is the dimensionality of the polarization propagation from the polar defect (for diluted polar point defects—e.g., grain corners—$d=3$; for isolated polar linear defects—e.g., grain edges—$d=2$; for isolated polar surfaces $d=1$). In our case of finite grains one could expect the main contribution to stem from the grain surfaces with $d=1$, implying that the experimental d should be certainly smaller than 3, or even than 2. The Raman strength of polar modes is obviously proportional to the total volume of polar regions (we assume incoherent scattering of individual grains) or averaged polarization, i.e., also to ξ^d, and our experiment yields $d\approx 1.6$ (Fig. 10) in reasonable agreement with our theoretical expectation.

A similar model can also be used to calculate the dielectric response function. The polarization is localized in the grain boundary layer of the characteristic thickness ξ whose permittivity $\varepsilon_{\mathrm{gb}}$ is connected with the stiffened soft mode response in these regions, while the grain interior permittiv-

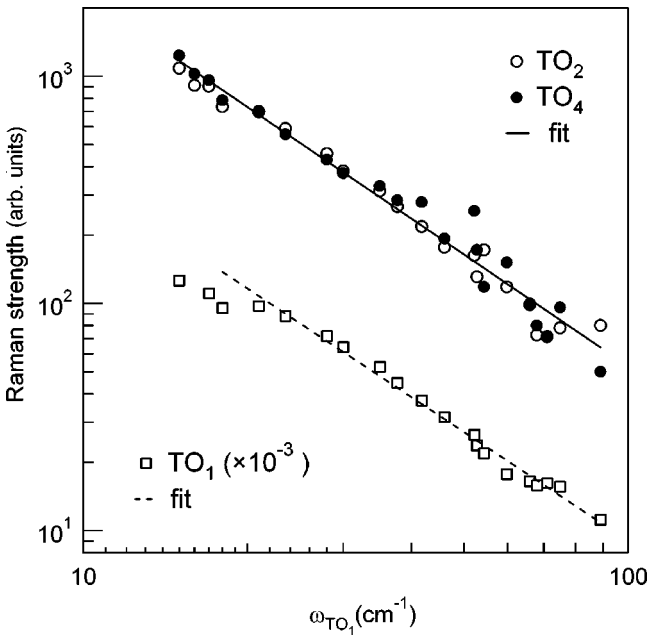

FIG. 10. Raman strengths of the IR modes as a function of the soft mode frequency ω_{TO1}. The fit to TO_2 and TO_4 strengths yields $I \propto \omega^{-1.63}$, the fit to TO_1 strength (taking as integral of the reduced Raman intensity from 12 to 100 cm^{-1}) excluding the data below 35 K (see text) yields $I \propto \omega^{-1.59}$.

ity is that of the single crystal $\varepsilon_{sc}(\omega)$. One can then use the brick model approach, successfully used for the discussion of dielectric properties in the case of $BaTiO_3$ ceramics.[49] In this model the effective dielectric response is estimated similar to a series combination of the bulk and surface layer (grain boundary) capacitances

$$\frac{1}{\varepsilon} = \frac{x}{\varepsilon_{sc}} + \frac{(1-x)g}{\varepsilon_{gb}}, \tag{3}$$

where x is the volume fraction of nonpolar grain interior, $(1-x) \propto \xi^d$ is the volume fraction of polar grain boundary layers, and g is a geometrical factor somewhat smaller than unity, which takes into account the small effect of grain boundaries in parallel with the grain bulk. In fact the permittivity varies near the grain boundary with the distance ξ and ε_{gb} represents its effective value. Considering approximately the permittivity (dielectric function) as given by the soft oscillator only (for simplicity, with the same damping and frequency of the LO mode over the whole grain), the inverse permittivity inside the grain is

$$\frac{1}{\varepsilon_{sc}} = \frac{\omega_{sc}^2 - \omega^2 + i\gamma_{sc}\omega}{\omega_{L1}^2 - \omega^2 + i\gamma_{L1}\omega}, \tag{4}$$

where ω_{sc} and γ_{sc} are TO_1 mode frequencies and dampings of the single crystal, respectively, while the effective permittivity ε_{gb} of the boundary is calculated as

$$\frac{1}{\varepsilon_{gb}} = \frac{1}{\xi}\int_0^{\xi} \frac{dz}{\varepsilon_{gb}(z)} = \frac{\omega_{gb}^2 - \omega^2 + i\gamma_{gb}\omega}{\omega_{L1}^2 - \omega^2 + i\gamma_{L1}\omega}, \tag{5}$$

where the effective frequency and damping of the soft mode in the grain boundary are $\omega_{gb}^2 = (1/\xi)\int_{D/2-\xi}^{D/2} \omega_{T1}^2(z)dz$ and $\gamma_{gb}^2 = (1/\xi)\int_{D/2-\xi}^{D/2} \gamma_{T1}^2(z)dz$, respectively. Then the overall effective response is still described by the damped oscillator with the soft mode frequency ω_{eff} shifted up to

$$\omega_{eff}^2 = \omega_{sc}^2 + 3\xi(g\omega_{gb}^2 - \omega_{sc}^2)/D > \omega_{sc}^2, \quad D \gg \xi \tag{6}$$

and with the damping increased to

$$\gamma_{eff} = \gamma_{sc} + 3\xi(g\gamma_{gb} - \gamma_{sc})/D > \gamma_{sc}. \tag{7}$$

The short-range forces, which appear near the grain boundaries as discussed in Ref. 48 in connection with the dynamics of a small ferroelectric particle, are neglected in the above model, but their inclusion can be shown to yield qualitatively the same result. Our experiment gives the lowest low-temperature value of ω_{TO1} about 15 cm^{-1} whereas its single domain crystal values are 7.8 and 16.5 cm^{-1} for the split E_u and A_{2u} components, respectively[50] (10.7 cm^{-1} as a weighted average). This is compatible with the reduced value of the low-temperature permittivity in ceramics compared with multidomain single crystals.

The question may be asked if the correlation length ξ is really much shorter than the grain size D down to the lowest temperatures. As no saturation of the IR mode Raman strengths in Fig. 9 is observed, it is likely so. The Raman strengths of the IR modes at lowest temperatures are comparable to those in STO single crystals doped with less than 1 at. % of Ca, where a field induced polarization of the order of 1 $\mu C/cm^2$ was observed.[23] It follows that our low-temperature averaged polarization P_{av} is of the same order and that the frozen polarization P_f should be much larger. A more quantitative estimate could be possibly done using ab initio calculations of the ideal grain boundaries.[47]

The hybridization of the TO_1 with the E_g mode (X mode) due to symmetry lowering is an additional effect which influences the dielectric response. It implies that P_f is perpendicular to the tetragonal c axis (as in Ca-doped crystals[23]). This supports the idea that the grain boundary dipole moment is not caused by random defects but rather by a specific atomic arrangement.[43–46] Moreover it implies that the tetragonal phase develops in a specific fixed orientation with respect to the grain boundary structure, since P_f exists in the cubic phase prior to the structural transition. This calls for microstructural studies of the tetragonal phase in a bicrystal. We believe that also in thin STO films the appearance of polar regions, which stiffens the TO_1 soft mode response and causes coupling between the TO_1 and structural soft modes, is an important reason for the smaller softening of the polar soft mode[8–11] and consequently lower permittivity.

Let us now comment on the comparison of IR and Raman responses in ceramics. As the grain size is much smaller than the polar phonon wavelengths, the IR response is directly comparable with the effective medium approximation used in our model even in the case of appearance of polar regions, which may produce local optical and dielectric anisotropy. Therefore the response is dominated by the slightly stiffened transverse polar frequencies as in the case of the soft mode discussed above.[51] On the other hand, the wavelengths of

first-order Raman active phonons are comparable to or smaller than the grain size so that the effective medium approximation is not valid. In this case, in addition to transverse polar modes the corresponding longitudinal modes and to a lesser extent all modes in between are also activated due to the polycrystalline character of the ceramic sample with polar grains of stochastic orientation.[52] This explains the much broader Raman response, particularly in the low-temperature and low-frequency range, where large TO-LO splitting of the polar soft mode causes an activation of a broad continuum which couples with the X mode and produces Fano type interferences with the TO_2 mode.

Finally, let us briefly discuss the MW losses in STO ceramics. Our model cannot explain the enhanced losses compared to single crystals[2,3] using the soft mode response only. The model can account for the decrease in MW permittivity, but does not yield increase in losses. Whereas in good single crystals the two-phonon absorption seems to explain the whole MW losses at least above T_a,[53] in ceramics additional losses due to grain-boundary scattering, proportional to the one-phonon density of states, may be activated. This yields additional losses proportional to frequency, which dominate in the higher GHz range,[2,54] whereas at lower frequencies relaxational contributions proportional to $1/\omega$ were also observed.[3,55] However, due to the limited frequency range the corresponding relaxation times could not be estimated. These losses, which point to charged point defects and/or fluctuations in the grain-boundary polarization P_f, have not yet been studied systematically. This would need dielectric studies on well defined samples at wide frequency and temperature range, which is quite a formidable task.

ACKNOWLEDGMENTS

We thank A. Jouck for preparing the ceramic samples and G. Wasse for metallography and microscopical studies. We appreciate the support of H. Lippert and M. Michulitz (ZCH, FZ Jülich) in performing the chemical analysis. The work was supported by the Grant Agency of the Czech Rep. (Project Nos. 202/01/0612 and 202/00/1187), Grant Agency of the Acad. Sci. CR (Project No. A1010918), Ministry of Education of the Czech Rep. (COST-OC 525.20/00), Deutsche Forschungsgemeinschaft (DFG) via GO 976/1 and Russian Foundation for Basic Research (Grant Nos. 99-02-16859 and 00-15-96773).

*Present address: Faculty of Physics, Rostov State University, Zorge 5, 344090 Rostov-on-Don, Russia.

[1] A. S. Barker, Jr. and M. Tinkham, Phys. Rev. **125**, 1527 (1962).
[2] G. Rupprecht and R. O. Bell, Phys. Rev. **125**, 1915 (1962).
[3] K. Bethe, Philips Res. Rep., Suppl. **2**, 1 (1970).
[4] O. G. Vendik, E. K. Hollmann, A. B. Kozyrev, and A. M. Prudan, J. Supercond. **12**, 325 (1999).
[5] H.-M. Christen, J. Mannhart, E. J. Williams, and C. Gerber, Phys. Rev. B **49**, 12 095 (1994).
[6] H.-CH. Li, W. Si, A. D. West, and X. X. Xi, Appl. Phys. Lett. **73**, 464 (1998).
[7] D. Fuchs, C. W. Schneider, R. Schneider, and H. Rietschel, J. Appl. Phys. **85**, 7362 (1999).
[8] I. Fedorov, V. Železný, J. Petzelt, V. Trepakov, M. Jelínek, V. Trtík, M. Čerňanský, and V. Studnička, Ferroelectrics **208-209**, 413 (1998).
[9] V. Železný, J. Petzelt, and K. Kämmer, J. Korean Phys. Soc. **32**, S1615 (1998).
[10] J. Petzelt, T. Ostapchuk, S. Kamba, I. Rychetský, M. Savinov, A. Volkov, B. Gorshunov, A. Pronin, S. Hoffmann, R. Waser, and J. Lindner, Ferroelectrics **239**, 117 (2000).
[11] A. A. Sirenko, C. Bernhard, A. Golnik, A. M. Clark, J. Hao, W. Si, and X. X. Xi, Nature (London) **404**, 373 (2000).
[12] S. Hoffmann and R. Waser, J. Phys. IV **8**, 221 (1998).
[13] R. Waser and O. Lohse, Integr. Ferroelectr. **21**, 27 (1998).
[14] S. K. Streiffer, C. Basceri, C. P. Parker, S. E. Lash, and A. I. Kingon, J. Appl. Phys. **86**, 4565 (1999).
[15] N. A. Pertsev, A. K. Tagantsev, and N. Setter, Phys. Rev. B **61**, R825 (2000).
[16] L. Ryen, E. Olsson, L. D. Madsen, X. Wang, C. N. Edvardsson, S. N. Jacobsen, U. Helmersson, S. Rudner, and L.-D. Wernlund, J. Appl. Phys. **83**, 4884 (1998).
[17] K. A. Müller and H. Burkard, Phys. Rev. B **19**, 3593 (1979).
[18] J. Dec, W. Kleemann, and B. Westwanski, J. Phys.: Condens. Matter **11**, L1 (1999).
[19] J. Petzelt, T. Ostapchuk, I. Gregora, S. Hoffman, J. Lindner, D. Rafaja, S. Kamba, J. Pokorný, V. Bovtun, V. Porokhonskyy, M. Savinov, P. Vaněk, I. Rychetský, V. Peřina, and R. Waser, Integr. Ferroelectr. **32**, 11 (2001).
[20] J. Petzelt, I. Gregora, I. Rychetský, T. Ostapchuk, S. Kamba, P. Vaněk, Y. Yuzyuk, A. Almeida, M. R. Chaves, B. Gorshunov, M. Dressel, S. Hoffmann-Eifert, and R. Waser, J. Eur. Cer. Soc. (to be published).
[21] R. Waser, T. Baiatu, and K.-H. Härdtl, J. Am. Ceram. Soc. **73**, 1645 (1990).
[22] J. G. Bednorz and K. A. Müller, Phys. Rev. Lett. **52**, 2289 (1984).
[23] W. Kleemann, A. Albertini, M. Kuss, and R. Lindner, Ferroelectrics **203**, 57 (1997).
[24] K. Hirota, J. P. Hill, S. M. Shapiro, G. Shirane, and Y. Fujii, Phys. Rev. B **52**, 13 195 (1995).
[25] R. Wang, Y. Zhu, and S. M. Shapiro, Phys. Rev. Lett. **80**, 2370 (1998).
[26] G. Kozlov and A. Volkov, in *Millimeter and Submillimeter Wave Spectroscopy*, edited by G. Gruner (Springer, Berlin, 1998), p. 51.
[27] D. Rafaja, V. Valvoda, A. J. Perry, and J. R. Treglio, Surf. Coat. Technol. **92**, 135 (1997).
[28] F. Gervais, in *Infrared and Millimeter Waves*, edited by K.J. Button (Academic Press, New York, 1983) p. 279.
[29] W. G. Nilsen and J. G. Skinner, J. Chem. Phys. **48**, 2240 (1968).
[30] P. A. Fleury, J. F. Scott, and J. M. Worlock, Phys. Rev. Lett. **21**, 16 (1968).
[31] J. Petzelt and V. Dvořák, J. Phys. C **9**, 1587 (1976).
[32] W. Taylor and A. F. Murray, Solid State Commun. **31**, 937 (1979).
[33] Na Sai and D. Vanderbilt, Phys. Rev. B **62**, 13 942 (2000).
[34] H. Vogt and G. Rossbroich, Phys. Rev. B **24**, 3086 (1981).
[35] G. Shirane and Y. Yamada, Phys. Rev. **177**, 858 (1969).

[36] I. Hatta, Y. Shiroishi, K. A. Muller, and W. Berlinger, Phys. Rev. B **16**, 1138 (1977).
[37] S. A. Hayward and E. K. H. Salje, Phase Transitions **68**, 501 (1999).
[38] B. Okai and J. Yoshimoto, J. Phys. Soc. Jpn. **39**, 162 (1975).
[39] M. Itoh, R. Wang, Y. Inaguma, T. Yamaguchi, Y.-J. Shan, and T. Nakamura, Phys. Rev. Lett. **82**, 3540 (1999).
[40] A. A. Sirenko, I. A. Akimov, J. R. Fox, A. M. Clark, H.-C. Li, W. Si, and X. X. Xi, Phys. Rev. Lett. **82**, 4500 (1999).
[41] H. Uwe, H. Yamaguchi, and T. Sakudo, Ferroelectrics **96**, 123 (1989).
[42] V. Janovec, V. Dvořák, and J. Petzelt, Czech. J. Phys., Sect. B **25**, 1362 (1975).
[43] M. M. McGibbon N. D. Browning, A. J. McGibbon, and S. Pennycook, Philos. Mag. A **73**, 625 (1996).
[44] N. D. Browning, H. O. Moltaji, and J. P. Buban, Phys. Rev. B **58**, 8289 (1998).
[45] F. Ernst, O. Kienzle, and M. Rhle, J. Eur. Ceram. Soc. **19**, 665 (1999).
[46] M. Kim, G. Duscher, N. D. Browning, K. Sohlberg, S. T. Pantelides, and S. J. Pennycook, Phys. Rev. Lett. **86**, 4056 (2001).
[47] S. Hutt, S. Kostlmeier, and C. Elsasser, J. Phys.: Condens. Matter **13**, 3949 (2001).
[48] I. Rychetský and O. Hudák, J. Phys.: Condens. Matter **9**, 4955 (1997).
[49] M. H. Frey, Z. Xu, P. Han, and D. A. Payne, Ferroelectrics **206-207**, 337 (1998).
[50] A. Yamanaka, M. Kataoka, Y. Inaba, K. Inoue, B. Hehlen, and E. Courtens, Europhys. Lett. **50**, 688 (2000).
[51] I. Rychetský, O. Hudák, and J. Petzelt, Phase Transitions **67**, 725 (1999).
[52] W. Hayes and R. Loudon, *Scattering of Light by Crystals* (Wiley, New York, 1978).
[53] A. K. Tagantsev, Zh. Eksp. Teor. Fiz. **86**, 2215 (1984).
[54] B. D. Silverman, Phys. Rev. **125**, 1921 (1962).
[55] I. M. Buzin, Vestn. Mosk. Univ. **18**, 70 (1977).